Computational Materials Science 172 (2020) 109333

Contents lists available at ScienceDirect

Computational Materials Science

journal homepage: www.elsevier.com/locate/commatsci

Lattice dynamics simulation using machine learning interatomic potentials

V.V. Ladygin[a,b,c,*], P.Yu. Korotaev[c,d], A.V. Yanilkin[b,c], A.V. Shapeev[a]

[a] Skolkovo Institute of Science and Technology, Skolkovo Innovation Center, Building 3, Moscow 143026, Russia
[b] Moscow Institute of Physics and Technology, Institutskiy Pereulok 9, Dolgoprudny, Moscow Region 141700, Russia
[c] Dukhov Research Institute of Automatics (VNIIA), Sushevskaya22, Moscow 127055, Russia
[d] National University of Science and Technology MISiS, Leninskiy prospect 4, Moscow 119991, Russia

ARTICLE INFO

Keywords:
Lattice dynamics
Anharmonicity
Machine learning
Moment tensor potentials

ABSTRACT

In this work, a machine-learning approach was applied to obtaining an interatomic potential for lattice dynamics properties calculation with accuracy close to the one of density functional theory (DFT). The computational efficiency of the potential allows one to access large time and length scales through molecular dynamics simulations. The use of active learning and an automatic training procedure greatly reduces the number of quantum-mechanical calculations for the training set. In order to estimate the accuracy of the obtained potentials, four materials Al, Mo, Ti and U with different phonon and thermodynamic properties were investigated. Phonon properties were calculated using the temperature dependent effective potential method. The potentials reproduce not only harmonic behavior but also anharmonic effects, as shown by the calculation of the third-order force constants. We found that machine-learning potentials reproduce quantum-mechanical data with high accuracy. Furthermore, the vibrational density of states was obtained via velocity autocorrelation function integration, which would be infeasible in direct quantum-mechanical simulations.

1. Introduction

Nowadays, applications of computer modeling in science is a rapidly growing area. For example, scientific modeling is used in all branches of physics, biology, and chemistry. The complexity of the modern problems that researchers face requires the simulation of realistic systems with the accuracy close to the experimental one. In particular, the broad range of such problems needs large time and length scale molecular dynamics (MD) simulations.

In order to perform an MD simulation, a model of interatomic interaction should be provided. An interatomic potential is, essentially, a function with a number of parameters fitted to certain reference data. For example, dislocation motion, diffusion of defects or shock-wave response, which are typical physical processes in metals, are often modeled with embedded atom method [1] or angular-dependent potentials [2]. A wide range of biological processes is simulated with the AMBER [3] and the CHARMM force fields. The ReaxFF [4] potential is used for the modeling of chemical processes, such as polymerization, isomerization, and catalysis. On the other hand, the potential energy surface (PES) could be accurately described by the numerical solution of Schrodinger's equation for the system. Density functional theory (DFT) is one of the approximations of such a model. It is very expensive for large time and length scale simulation in the context of quantum molecular dynamics [5].

For this reason, research towards efficient methods that could describe PES with high accuracy is one of the major directions of modern computational material science. In particular, machine-learning approaches have proved themselves to be more flexible [6,7] and to reproduce PES better than force fields with a certain functional form and work much faster and scale better than *ab initio* methods.

Despite the fact that machine learning became a widely-used tool in all areas of science a long time ago, especially in physics [8] and chemistry [9], it was applied mostly for specific classification problems, such as spectra peaks and binding sites of biomolecules recognition [10,11] or determination of quantitative structure-activity relationships (QSARs) [12]. Currently, according to this trend, machine learning started to find new, more profound applications in computational material science and chemistry. For example, similar to QSAR and drug design methodologies, machine learning was utilized as a tool for the determination of materials structure-properties relationship [13]. Furthermore, machine learning can also be used to obtain accurate interatomic potentials which became the area of intensive research.

One of the first machine-learning techniques applied for interatomic potential construction was neural networks [14,15]. Recent progress in this field shows the ability to fit sophisticated potential energy surfaces of solid water [16] making an emphasis on anharmonic behavior

* Corresponding author at: Skolkovo Institute of Science and Technology, Skolkovo Innovation Center, Building 3, Moscow 143026, Russia.
E-mail address: vladimir.ladygin@skoltech.ru (V.V. Ladygin).

https://doi.org/10.1016/j.commatsci.2019.109333
Received 31 July 2019; Received in revised form 3 October 2019; Accepted 4 October 2019

reproduction. Another approach is interatomic potentials based on Gaussian process regression, GAP, proposed in [17]. In several years, these potentials have been applied to a broad range of physical problems [6,18,19]. Furthermore, recently they were used to the study of Si and Zr lattice dynamics [20,21]. However, in [22], authors took only harmonic part of the vibrational spectrum into consideration. In [20] it was discussed that GAP potential fitted on the database with the limited number of near-equilibrium structures is not sufficient for the reproduction of anharmonic behavior of Si. On the other hand, in [16,21] authors have shown the ability to accurately reproduce anharmonic behavior of PES, but it required a huge manually constructed training set of representative structures.

In our work, we have chosen the moment tensor potential (MTP) first proposed in [23]. The potential functional form is based on describing the shells of atoms of local atomic environments by their moments of inertia—hence its name. MTP benefit from the active-learning algorithm developed in [24,25] that assemble the training set on-the-fly by adding atomic configurations on which extrapolation is attempted. Such a combined active-learning and MTP algorithm has been used to study elastic properties in a multi-principal element alloy [26], diffusion of point defects [27], and chemical reactions [28]. However, it has not been studied how well MTPs or other machine-learning potentials reproduce anharmonic effects of lattice dynamics of single-component systems with different chemistry.

In this paper, we focus on lattice dynamics, as one of the basic phenomena in solids. The lattice dynamics defines such properties of a system as vibrational density of states and dispersion curves. We use MTP to calculate the harmonic and anharmonic behavior of a number of different single-component systems and compare them to reference DFT results.

It should be noted that there are several methods that allow one to obtain vibrational properties from *ab initio* calculations which vary by the level of approximation. For example, small-displacement method and method of self-consistent *ab initio* lattice dynamics (SCAILD) [29] use quasi-harmonic model for vibrational band structure calculation. The effects of anharmonicity can be taken into account by perturbation corrections [30] and by the method of temperature dependent effective potential (TDEP) [31,32], to name a few.

An accurate way to calculate the vibrational density of states is Fourier transform of velocity autocorrelation function [33,34]. This approach allows one to implicitly take into account anharmonic effects up to all orders but requires large time and length scales. For this reason, the construction of the accurate potential with machine-learning technique is essential for such calculations.

In this work, crystalline of face-centered cubic (fcc) aluminum, body-centered cubic (bcc) molybdenum, bcc titanium and uranium phases at finite temperature were investigated. The elements were explored here, firstly, in the order of anharmonic behavior increasing and secondly in order of growing complexity of their PES which is an issue for pure DFT calculation. Aluminum was chosen as an element with little anharmonic effects in the potential energy surface and relatively simple electronic structure. Molybdenum and titanium were chosen as well-studied materials with pronounced anharmonic effects. Uranium was taken as the material with complex and anharmonic potential energy surface, which is poorly described by DFT. Moreover, to the authors' knowledge, the vibrational density of states of the element was not investigated in previous studies. Furthermore, we emphasize that bcc-Ti and bcc-U are temperature-stabilized due to strong anharmonicity.

For each element its vibrational spectrum was compared with the *ab initio* one. For this purpose, TDEP was used. This tool can be applied both to the *ab initio* and MTP models and allows one to take into account anharmonic effects explicitly by the third-order force constants calculation.

The main goal of the work is to study the accuracy with which MTP describes the DFT model in the context of phonon and thermodynamic properties reproduction. We find that for a range of single-component systems the error between DFT and MTP is less than the error between DFT and experimental data. We also show that with automatic training database selection MTP is able to capture the anharmonic effects with high accuracy. In Section 2 the details of applied interatomic potential are introduced. In Section 3 the computational details are given. In Section 4 we present the computations of the phonon properties with anharmonic effects shown directly by the third-order force constants calculation. The results are compared to pure DFT calculations in Section 4.1. Finally, phonon dispersion curves, vibrational density of states, the values of entropy and vibrational free energy are presented in Sections 4.2, 4.2.3 in comparison with existing experimental results.

2. Moment tensor potential (MTP)

In this work, lattice dynamics computations were performed with the moment tensor potential (MTP). In this model, the total interaction energy of the structure is presented as a sum of atomic contributions $V(\boldsymbol{r_i})$. Here $\boldsymbol{r_i}$ is the atomic neighborhood encoded in the set of vectors connecting atom i with the neighboring atoms j, $\boldsymbol{r_i} = \{r_{ij}\}$. Each contribution $V(\boldsymbol{r_i})$ is expanded as a linear combination of basis functions $B_k(\boldsymbol{r_i})$. Thus, the total energy of a configuration x could be written as

$$E(x) := \sum_{i=1}^{N} \sum_{k} \theta_k B_k(\boldsymbol{r_i}), \tag{1}$$

where N is the number of atoms of the configuration x, θ are the adjustable parameters to be found by minimizing the difference between $E(x)$ and the DFT energy, together with forces and virial stresses, on a training set of configurations x. The basis functions are constructed as different contractions of moment tensor descriptors of atomic environments

$$M_{\mu,\nu}(u) := \sum_{i=1}^{n} \left| u_i \right|^{2\mu} u_i^{\otimes \nu}(u), \tag{2}$$

where integers $\mu, \nu \geqslant 0$ index different descriptors, and $u^{\otimes \nu}$ is the Kronecker product of ν copies of the vector u. This functional form respects all the physical symmetries. The details can be found in [23,25].

There are two methodologies for assembling a training set. The first one is passive learning, the potential is trained using the whole dataset of structures processed by the reference model. This approach requires large dataset of reference model (DFT, in our case) calculations in order to cover the phase space of the system. Learning on-the-fly or active learning (AL) methodology enables a potential to be automatically fitted only on those configurations on which significant extrapolation is detected. In this case, only a few configurations required for the phase space of the system description are processed by the reference model. This approach significantly decreases the number of DFT calculations required for potential training.

3. Details of computation

DFT model implemented in the VASP code [35,36] was used as reference potential in training procedure and for calculation of DFT trajectories. Molecular dynamics simulations were performed using the LAMMPS code [37]. MTP, implemented as a LAMMPS plugin, was used as an interatomic potential. For the force constants calculations the TDEP code [31,32] was exploited.

3.1. DFT calculations

DFT calculations were performed as a part of potential training to obtain reference energies, forces, and stresses. The computations were done with the projector-augmented wave (PAW) method and by the means of generalized gradient approximation (GGA) according to the

Table 1
Average (index *avg*) difference in potential energy per atom $U/3kT$ and relative (index *rel*) difference in forces F between trained machine-learning potential and reference model. The error in potential energy of MTPs is small compared to the DFT model.

Element	T, K	Lattice type	a, Å	$U_{avg}/3kT$, %	F_{rel}, %
Al	775	fcc	4.11	0.1	3
Mo	300	bcc	3.15	0.1	3
Mo	1500	bcc	3.166	0.3	3
Ti	1500	bcc	3.3257	0.6	25
U	1350	bcc	3.49	1.3	27

parametrization of Perdew, Burke, and Ernzerhof (PBE) for the exchange-correlation energy. The cutoff energy chosen for the plane wave is 320 eV for Al, 300 eV for Mo, 250 eV for Ti and 330 eV for U. The k-point mesh was $4 \times 4 \times 4$ ($3 \times 3 \times 3$ for U) for the $3 \times 3 \times 3$ conventional supercell. Moreover, *ab initio* MD simulations were performed for the NVT ensemble. The supercell and calculation parameters were chosen to be the same as in the training procedures.

3.2. Training procedure

Learning on-the-fly was used in the training procedure in order to minimize the number of DFT calculations. The MD run was performed for the NVT ensemble during 70000 steps (the time step was 1 fs); the temperature and lattice constant (a is in Table 1) were chosen the same as the experimental ones [38–41]. Dependence of the number of *ab initio* calculations on the MD run step in double logarithmic scale is shown in Fig. 1.

It is evident from the figure that on-the-fly training significantly decreases the number of DFT calculations compared to the passive learning. The number of configurations requested to be computed by the *ab initio* model is approximately 100 for Al, Mo and is around 300 for Ti and U.

The average difference in the potential energy per atom divided by $3kT$ and the relative difference in forces between the reference model and MTP is shown in Table 1. The highest absolute energy error divided by characteristic thermal vibrational energy of the potential is equal to 1.3%. From this, we can conclude that potential accurately describes the potential energy surface of the system compared to the reference model. The maximum error of forces is 27%. This error is large, but later it will be shown how it influences the second and the third-order derivatives values. From the difference in the potential energy value, it could be concluded that our calculations via machine-learning potential approach reflect well the behavior of the *ab initio* model.

3.3. TDEP calculation

The TDEP method is used to verify how MTP reproduces force constants of the system with respect to the DFT calculations. In this method [31,32], a model Hamiltonian is used to fit the Born-Oppenheimer molecular dynamics potential energy surface at finite temperature. The obtained effective potential is applied for the interatomic force constants (IFCs) calculation. IFCs are then used for the calculations of the vibrational properties.

To validate the accuracy of the trained potential, an MD run was performed (20000 steps, one step was 0.5 fs) for the $3 \times 3 \times 3$ conventional cell. During every 100 steps, the structures for the TDEP fitting were selected. Furthermore, TDEP was fitted on configurations uniformly selected from *ab initio* MD trajectories (Section 3.1). The calculated vibrational density of states and dispersion curves were compared with each other. The TDEP software also allowed calculating third-order force constants which are attributed to the finite phonon lifetime. Using this calculations we computed the broadening and shifting of the vibrational spectrum for MTP and DFT. Finally, comparing the obtained spectrum we can establish that MTPs reproduce accurately anharmonic effects.

3.4. VACF calculation

Thermodynamic properties such as vibrational entropy and free energy play a significant role in the determination of system stability at finite temperatures. These qualities can be calculated directly from the vibrational density of states. In order to reproduce the vibrational density of states with anharmonic effects the velocity autocorrelation function (VACF) method is used. VACF, $\langle v(t)|v(0)\rangle$, can be calculated explicitly from molecular dynamics simulation. Vibrational density of states is obtained by the Fourier transform of the VACF [33],

$$g(\nu) = \int_0^\infty \cos 2\pi\nu t \frac{\langle \overline{v(0)v(t)} \rangle}{\langle \overline{v(0)}^2 \rangle} dt, \tag{3}$$

where ν is the vibrational frequency, and the average $\langle \bar{\cdot} \rangle$ is taken over all atoms. The advantage of such a method is its high accuracy in vibrational density of states description. On the other hand, to achieve this accuracy, calculation for large system should be performed, so one can use *ab initio* molecular dynamics only for very approximate calculations [5].

The trained potential was used for the supercell ($20 \times 20 \times 20$) MD simulation with periodic boundary conditions in all directions. The system was equilibrated using MD in the NVT ensemble for 4 ps. After that, calculations of VACF in the NVE ensemble for another 4 ps were performed. As shown in [42], the characteristic time of VACF decay in the considered systems is about 1 ps. Finally, the vibrational density of

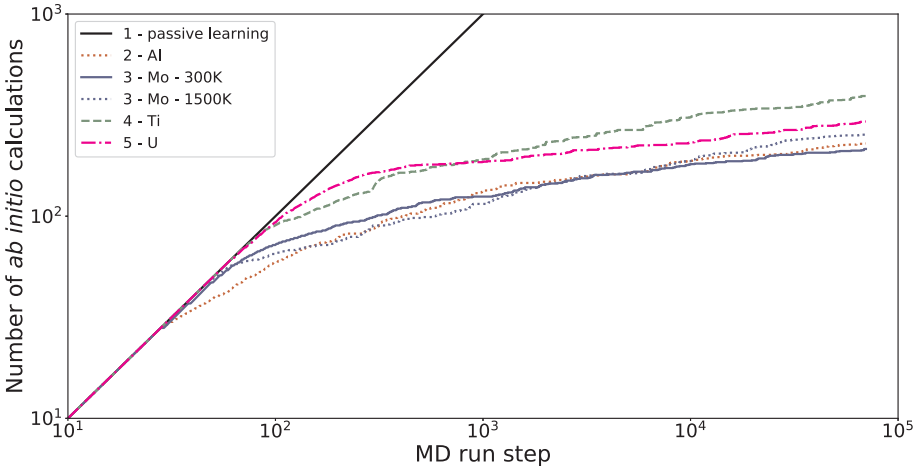

Fig. 1. Dependence of the number of configurations processed by DFT on the whole number of structures in the MD run: 1: passive learning, 2: fcc Al (T = 775 K), 3: bcc Mo (T = 300 K and T = 1500 K), 4: bcc Ti (T = 1500 K), 5: bcc U (T = 1350 K). We see that active learning gradually reduces number of configuration processed by DFT compared to passive learning.

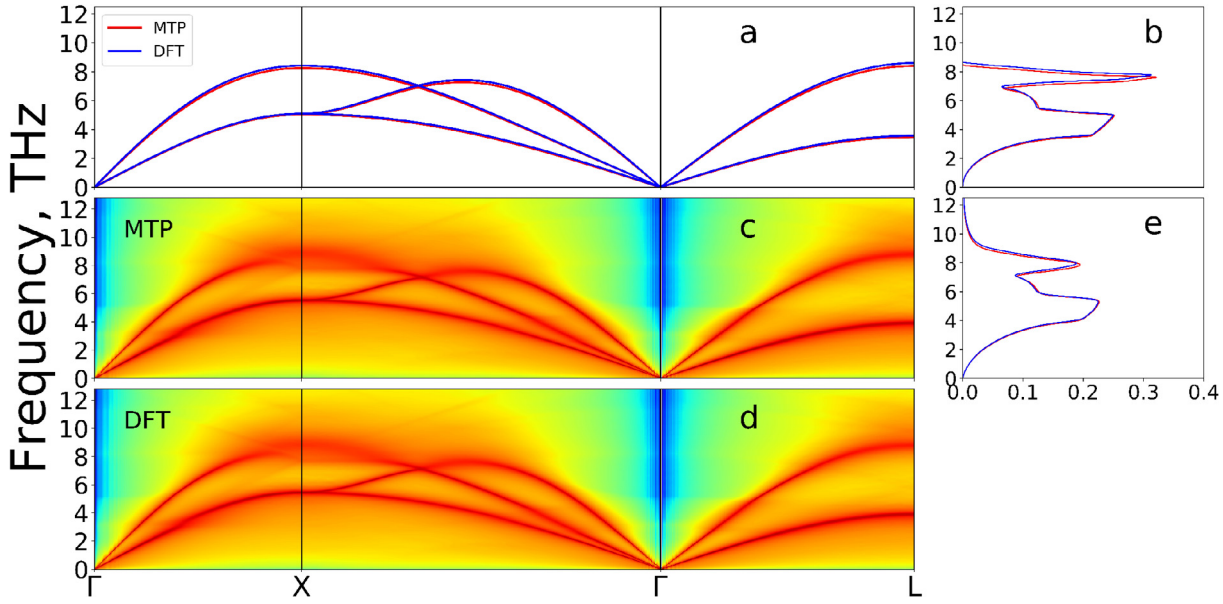

Fig. 2. Vibrational spectrum for fcc aluminum, including the effects of anharmonic phonon broadening and shifting, at 775 K: a, b: phonon dispersion curve and phonon density of states for MTP and DFT not taking into account the third-order force constants; c, d: vibrational spectrum for MTP and DFT with direct anharmonicity described by the third-order force constants; e: vibrational density of states for MTP and DFT with the broadening effect (force constants, vibrational spectrum and density of states are calculated via TDEP). One can see that the MTP and DFT curves are in perfect correspondence.

states calculation was performed using (3).

4. Results and discussion

4.1. MTP and DFT comparison

As it is known, anharmonic behavior is best captured with increasing temperature. For this reason, high temperature conditions were chosen for all elements.

4.1.1. Aluminum

The calculated vibrational spectrum for Al at T = 775 K is plotted in Fig. 2. As it is evident from Fig. 2(a) and (b) that harmonic behavior reproduces accurately by MTP. Furthermore, Fig. 2(c) and (d) show clearly that the anharmonic part of the spectrum agrees well when compared to the DFT model. For example, this fact can be recognized by looking at anharmonicity in the X point region. Furthermore, this effect is in correspondence with the broadening of the vibrational spectrum from 10 to 12 THz. This shows that the MTP potential in the case of Al reflects the behavior of the DFT model with high accuracy.

4.1.2. Molybdenum

The calculated vibrational spectrum for Mo at T = 1500 K is plotted in Fig. 3. The reference vibrational spectrum of DFT presented in Fig. 3(c) has small broadening effects. This fact is also evident from the vibrational spectrum obtained via the machine-learning potential (Fig. 3(d)). Thus, the results of computations using MTP and DFT are in good agreement with each other. Broadening of the phonon dispersion curves and corresponding broadening of vibrational density of states (Fig. 3(e)) are also captured by MTP with high accuracy.

4.1.3. Titanium

In the present work, the vibrational properties of Ti bcc phase are also studied. It should be noted that the bcc phase of Ti is not stable at low temperature. This leads to more complicated lattice dynamics. As a consequence, the reproduction of bcc Ti behavior is a more challenging test for MTP. The calculated vibrational spectrum for bcc Ti at T = 1208 K is plotted in Fig. 4. Phonon dispersion curves calculations by MTP and DFT are in good agreement with each other. The clear anharmonic effect is the broadening of the spectrum near the H point (Fig. 4(c)), which leads to the broadening of vibrational density of states up to 8 THz (Fig. 4(e)). This feature is well-reproduced by MTP.

4.1.4. Uranium

The study of uranium is a challenging problem due to its complicated potential energy surface and huge anharmonic effects. Also, the bcc phase of uranium is not stable at a low temperature similar to the Ti case in Section 4.1.3. The calculated vibrational spectrum for γ-U at high temperature (T = 1113 K) are plotted in Fig. 5. The results obtained with MTP and the *ab initio* model are in a good agreement with each other.As it was shown in Section 3.2 the force error of MTP compared to DFT for Ti and U is larger than for Al and Mo. However, the anharmonic structure of vibrational spectrum of these elements is in an excellent agreement (Fig. 4(c), (d), Fig. 5(c), (d)). In particular, anharmonicity near the P and N points, which leads to the broadening of the spectrum from 2.5 to 3.5 THz, is well reproduced by MTP. The huge anharmonic effects clearly seen in the DFT spectrum (Fig. 5)) and its corresponding plot obtained by MTP (Fig. 5(c)) allow us to conclude that MTP captures the behavior of DFT with high accuracy.

4.2. MTP and experimental data comparison

In the previous section, we compared the MTP and DFT data. In this section, we study how MTP reproduces lattice dynamics with respect to experimental data. The difference between the MTP and experimental data is compared to the difference between the MTP and DFT data. The choice of materials' phases and temperatures was based on the availability of the experimental data. To the authors' knowledge, there were no experiments with the direct measurements of vibrational density of states for bcc titanium and vibrational spectrum for high-temperature fcc Al (T = 775) and bcc U. For this reason, vibrational density of states were compared in the cases of Al and U and phonon dispersion curves in the cases of Mo and Ti. Also, materials' phases and temperatures were chosen to explore how MTP reproduces anharmonic behavior with respect to the experiment. For this reason, Al at high temperature was studied and materials with anharmonic behavior in the vibrational spectrum such as Mo, Ti, and U were investigated.

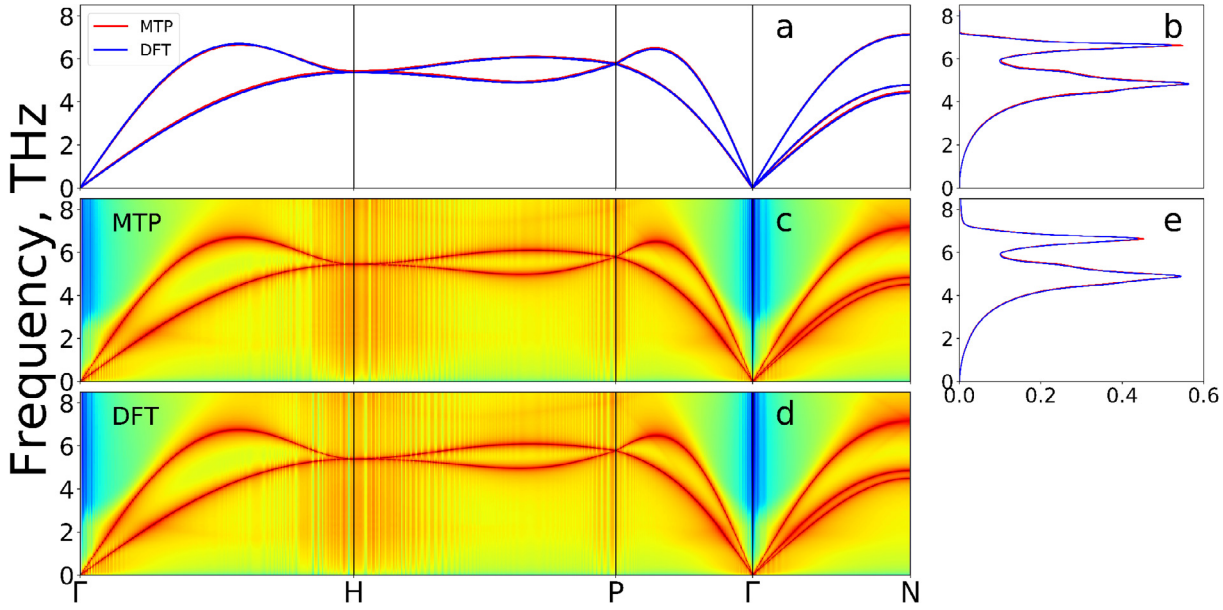

Fig. 3. Vibrational spectrum for bcc molybdenum at 1500 K: a, b: phonon dispersion curve and phonon density of states for MTP and DFT not taking into account the third-order force constants; c, d: vibrational spectrum for MTP and DFT with direct anharmonicity described by the third-order force constants; e: vibrational density of states for MTP and DFT with the broadening effect. The plot shows an excellent correspondence between the MTP and DFT curves.

4.2.1. Aluminum and uranium

Vibrational density of states (VDOS) of fcc Al at T = 775 K obtained via the VACF analysis is plotted in Fig. 6(a) along with the experimental values of Stedman and Nilsson [43]. The calculated VDOS agrees with the experimental one. As one can see, not only the position of the peaks but also the broadening is reproduced by MTP. This is because of a good description of the vibrational properties of aluminum by DFT. The obtained results are also in agreement with anharmonicity in the vibrational spectrum presented in Fig. 2 c which leads to the broadening of the density of states up to 12 THz.

In the case of uranium, there were several attempts to investigate its vibrational spectrum at finite temperature. For example, its band structure was investigated using a combination of DFT and SCAILD with full potential linear muffin-tin orbitals model (FPLMTO) [44]. More recently, this element was investigated using TDEP with PAW [45]. Both approaches TDEP and SCAILD are effective-harmonic models. Such tools, however, can reproduce anharmonic effects such as broadening of the spectrum only up to a finite order. In our work, the computational efficiency of the potential allowed us to obtain the vibrational density of states using an MD simulation by analyzing VACF, which would be infeasible for the pure DFT calculations. The advantage of this approach is that it properly takes into account anharmonic effects. The calculated vibrational density of states for bcc U at high temperature (T = 1113 K) and the experimental values from [46] are plotted in Fig. 6(b).

One can see that the obtained results differ from the experimental

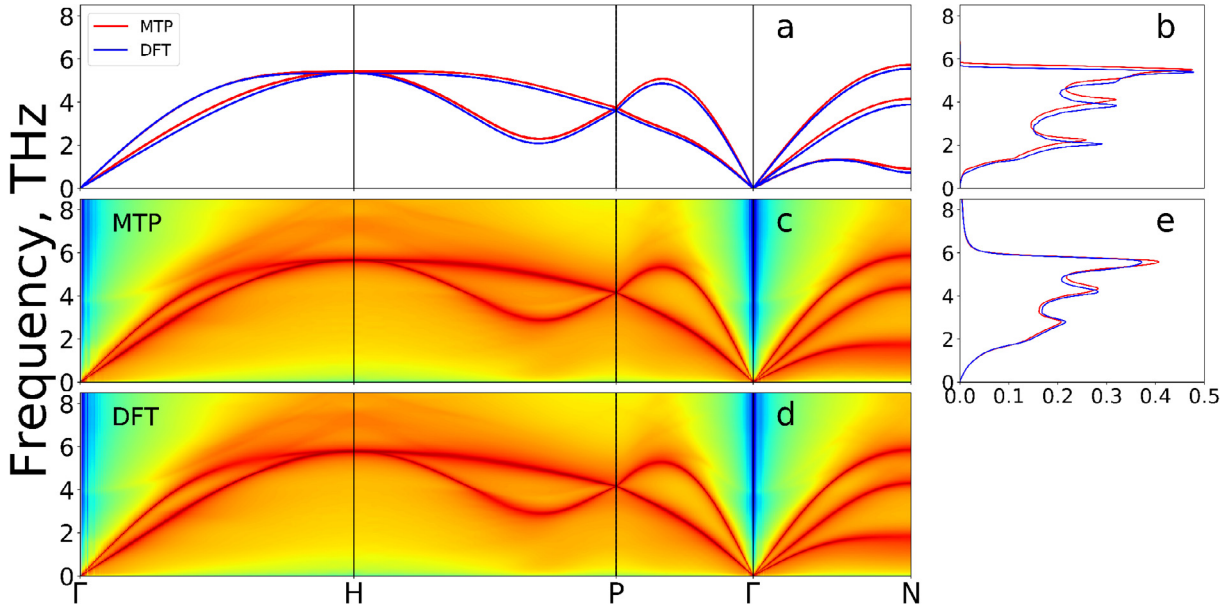

Fig. 4. Vibrational spectrum for bcc titanium at 1208 K: a, b: phonon dispersion curve and phonon density of states for MTP and DFT not taking into account the third-order force constants; c, d: Vibrational spectrum for MTP and DFT with direct anharmonicity described by the third-order force constants; e: vibrational density of states for MTP and DFT with the broadening effect. Anharmonic effect near the H point is well-reproduced by MTP.

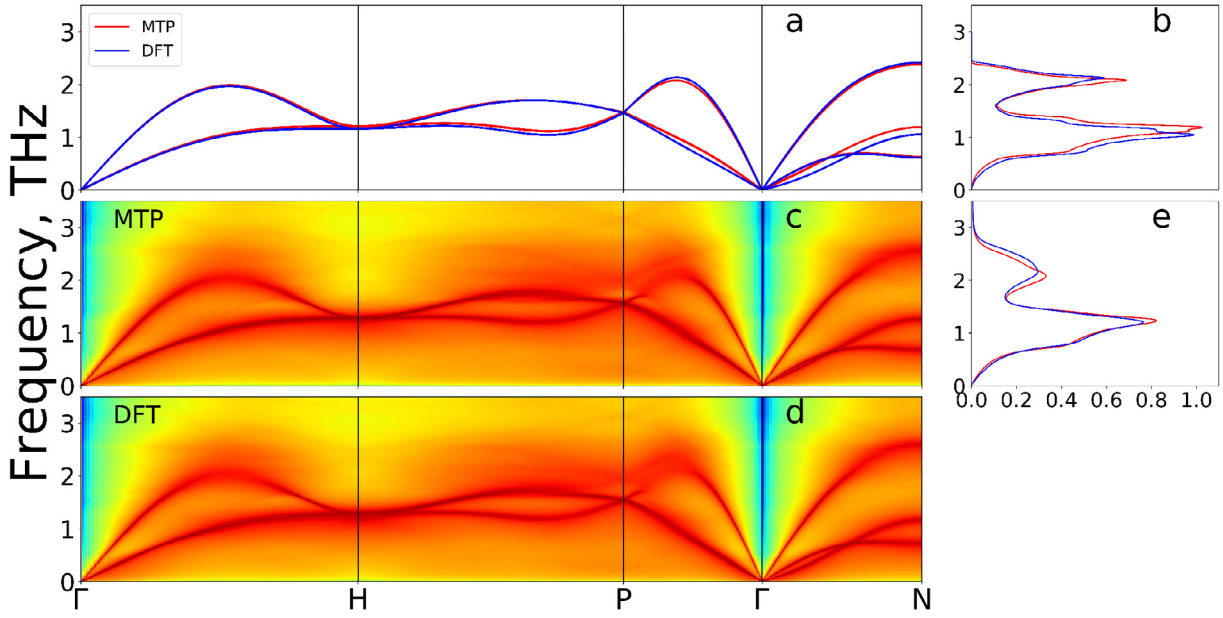

Fig. 5. Vibrational spectrum for bcc uranium at 1113 K: a, b: phonon dispersion curve and phonon density of states for MTP and DFT not taking into account the third-order force constants; c, d: vibrational spectrum for MTP and DFT with direct anharmonicity described by the third-order force constants; e: vibrational density of states for MTP and DFT with the broadening effect. One can see that U has the highest anharmonicity among the investigated materials but MTP is still in a very good agreement with DFT calculations.

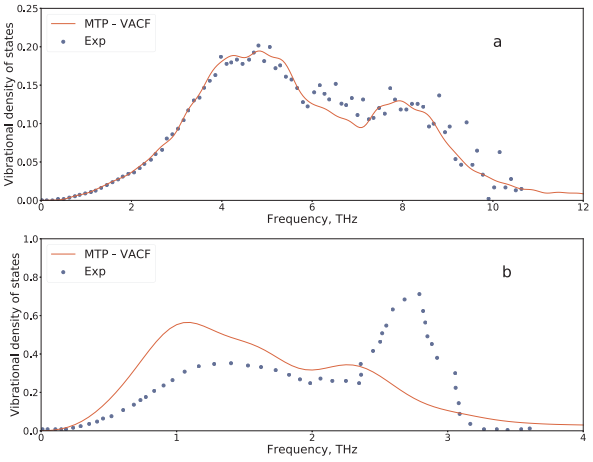

Fig. 6. Vibrational density of states for **(a)**: fcc Al at 775 K and **(b)**: bcc U at 1113 K: Exp: experimental data from [43,46], MTP - VACF: calculations via VACF using MTP. The plot demonstrates that calculations performed with MTP reflect the position of the peaks and broadening compared to the experimental data in Al case. For U, the plot demonstrates that MTP inherits the DFT model drawbacks in the description of uranium comparing to experimental data.

data. It is reflected in peak positions and broadening effects. However, from Fig. 5 it is evident that MTP reproduces DFT with high accuracy. This means that the DFT model has issues with the description of real uranium lattice dynamics as it was shown in [44,47,48] and MTP inherits such drawbacks being an accurate approximation of the reference model. Therefore, it could be concluded that in the case of U, MTP reflects behavior of DFT much better than DFT describes the experiment.

4.2.2. Molybdenum and titanium

The calculated phonon dispersion curves for Mo and the experimental values measured by the means of neutron spectrometry from [49] are plotted in Fig. 7(a). The dispersion curves were not reproduced accurately by MTP compared to the experimental data, but the reference DFT model (Fig. 3(a)) establishes a similar problem in the region that is also shown in [50]. This brings us to the conclusion that our machine-learning potential reproduces its reference model better than the reference model describes the experiment.

The calculated phonon dispersion curves for bcc Ti and the experimental values from [51] are plotted in Fig. 7(b). The difference between the obtained and experimental results can be viewed as a drawback of DFT in the description of Ti (Fig. 4(a)). Furthermore, looking back at Fig. 4(c), one can see that the huge broadening of the vibrational spectrum near the H point is in agreement with the broadening of the spectral lines obtained in the scattering experiment presented in [51].

4.2.3. Free energy calculation

In the previous sections, we have compared the vibrational spectrum and vibrational density of states calculated using MTPs with respect to DFT and the experimental data. The next step is to investigate how the obtained potentials reproduce thermodynamic properties such as entropy and vibrational free energy. These properties determine the stability of the structure at finite temperature. In Table 2 the results of the total entropy S_{TDEP} and vibrational free energy F_{vib} obtained via TDEP are presented. For such a comparison with the experimental data, the entropy S_{VACF} was calculated from the vibrational density of states obtained via VACF. The accuracy of such an approach is discussed in [34].

The difference in entropy between the trained potential and the reference model is around 10^{-2} for Al and Mo, approximately $2{\cdot}10^{-2}$ k_B/atom for Ti, and $2{\cdot}10^{-1}$ k_B/atom for U. The maximal discrepancy in entropy with respect to the experimental data is around $9{\cdot}10^{-1}$ k_B/atom for uranium. This error comes from a complex and anharmonic potential energy surface of uranium which leads to inaccuracy of the DFT model. Furthermore, the results are in agreement with the softening of the VDOS, presented in Fig. 6. The error for Al, Mo, and Ti is less or of the order of 10^{-1} k_B/atom which is as large as the difference between MTP and DFT. The difference in the free energy computation between the trained potential and the reference model is 0.1% of average thermal vibrational energy or less for Al, Mo, and Ti, and 7% for U. This values are comparable to the energy error of MTP with respect to the reference model. Overall, the error of the MTP data with respect to DFT data is

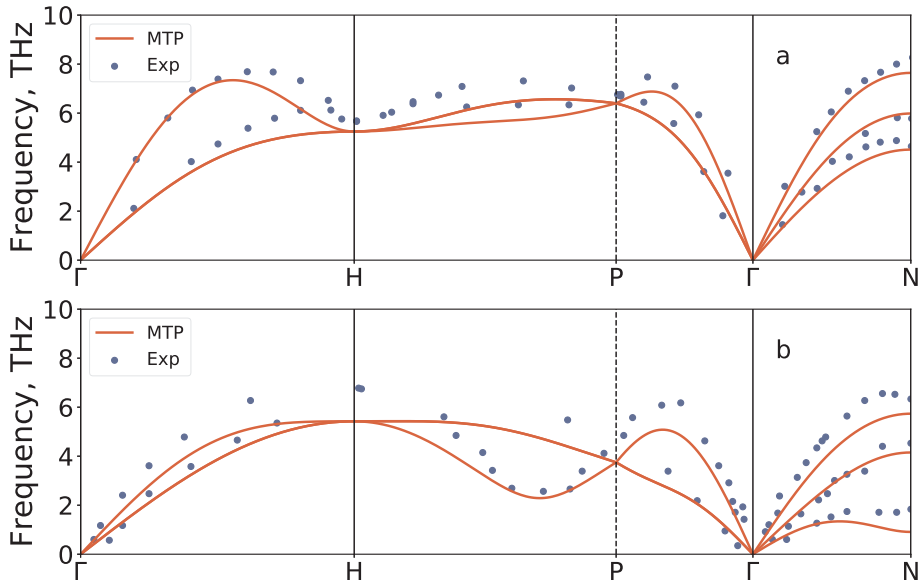

Fig. 7. Phonon dispersion curves along symmetry directions for **(a)**: bcc molybdenum at 300 K; **(b)**: bcc titanium 1208 K: Exp: experimental data from [49,51], MTP – TDEP: calculations via TDEP using MTP. We attribute the deviation from the experimental data to the quality of the DFT model.

much less than the error of DFT with respect to experimental results for elements with different complexity of PES and anharmonic behavior. This brings us to the conclusion that MTP has a high accuracy for the reproduction of the lattice dynamics of single-component systems compared to the DFT model.

5. Conclusion

In this paper, moment tensor potentials (MTPs) were used to combine the accuracy of *ab initio* calculations and efficiency of molecular dynamics. The potentials are constructed based on DFT data. Furthermore, active learning, used in the training procedure, allowed us to decrease the number of quantum computations by several orders of magnitude during the training procedure. Furthermore, the usage of MTP reduces calculation time compared to VASP by several orders of magnitude. The CPU time spent on the molecular dynamics step is of the order of 0.1 ms per atom per core for MTP and does not depend on the atomic type. For DFT calculations this value ranges between ten and thousand seconds per atom per core, depending on the atom type. Scaling of computational complexity with the number of atoms is N for the MTP potential and between N^2 and N^3 for the VASP calculations. As a result, calculations using MTP greatly reduce the total calculation time and allows one to perform large time- and length-scale simulations without significant loss in accuracy.

In order to estimate the quality of our machine-learning potential, we explored the lattice dynamics of four elements, Al, Mo, Ti, and U, with different complexity of the potential energy surfaces and anharmonic behavior. The accuracy of MTP with respect to the quantum-mechanical data was assessed. To study the accuracy, phonon dispersion curves and phonon density of states of the elements were obtained with an effective harmonic model. Moreover, the comparison of anharmonic behavior of MTP and DFT was performed by calculating the third-order force constants.

Additionally, the results of MTP were compared to the existing experimental results. This was done in order to have a benchmark that could be used to quantify the accuracy of MTP with respect to DFT. The phonon dispersion curves for Mo and Ti and the vibrational density of states for Al and U were obtained with MTP. The accuracy of the MTPs with respect to experiment depends on the accuracy of the DFT model: the error between MTP and DFT is much less than the difference between MTPs and the experimental data.

Furthermore, the difference in the entropy and vibrational free energy between the trained potentials and DFT was estimated. Again, this value was smaller than the error of DFT compared to the experimental results. Also, this error was lower than the difference of values obtained with the two methods used in the study, TDEP and VACF analysis. Moreover, it was shown that the vibrational free energy difference is of the order of the potential energy error.

To the best of our knowledge, for the first time we have shown that a machine-learning potential, MTP, was able to take into account anharmonicity of the potential energy surface when automatically fitted on-the-fly on a relatively small number of quantum calculations. The efficiency of the potential allowed us to perform large MD simulations reproducing anharmonicity for a number of materials with different chemistry. Moreover, it was shown that MTP captured the behavior of the DFT model with higher accuracy than that of DFT as compared to the experimental data.

The possible field of future research is the study of lattice dynamics

Table 2
Total entropy S, vibrational free energy F_{vib} and difference in free energy between MTP and DFT denoted as ΔF. The index "DFT" corresponds to calculations using DFT, the index "TDEP" is related to results obtained via TDEP and the index "EXP" denotes experimental results. One can see that difference in entropy between MTP and DFT is less (for the Mo case equal) than the difference between the DFT model and experiment.

	T, K	$S^{\text{MTP}}_{\text{TDEP}}$ k_B/atom	$S^{\text{DFT}}_{\text{TDEP}}$, k_B/atom	$F^{\text{MTP}}_{\text{vib}}$, meV/atom	$F^{\text{DFT}}_{\text{vib}}$ meV/atom	$\Delta F 3kT$, %	$S^{\text{MTP}}_{\text{VACF}}$ k_B/atom	S^{EXP}, k_B/atom
Al	775	6.251	6.263	−235.2	−235.9	0.1	6.338	6.332
Mo	300	3.750	3.758	−9.03	−9.04	0.1	3.800	3.451
Ti	1208	9.770	9.785	−611.8	−613.3	0.5	9.551	9.041
U	1113	13.249	13.432	−820	−840	7	12.970	11.761

of multicomponent systems, MTP has shown a good performance on multicomponent metallic systems [52,26] and promising results on a system with covalent/ionic bonding [53].

Acknowledgments

The work was supported by the Russian Science Foundation (Grant No. 18-13-00479).

Data availability

The processed data required to reproduce these findings are available to download from [https://drive.google.com/open?id=1oFrVb1-lOj7_ieeSffKZSl9QS-0PfOgu]. The raw data required to reproduce these findings cannot be shared at this time due to technical or time limitations.

Appendix A. Supplementary data

Supplementary data associated with this article can be found, in the online version, athttps://doi.org/10.1016/j.commatsci.2019.109333.

References

[1] R. Johnson, D. Oh, Analytic embedded atom method model for bcc metals, J. Mater. Res. 4 (5) (1989) 1195–1201.
[2] Y. Mishin, A. Lozovoi, Angular-dependent interatomic potential for tantalum, Acta Mater. 54 (19) (2006) 5013–5026.
[3] C.J. Dickson, B.D. Madej, Å.A. Skjevik, R.M. Betz, K. Teigen, I.R. Gould, R.C. Walker, Lipid14: the amber lipid force field, J. Chem. Theory Comput. 10 (2) (2014) 865–879.
[4] A.C. Van Duin, S. Dasgupta, F. Lorant, W.A. Goddard, Reaxff: a reactive force field for hydrocarbons, J. Phys. Chem. A 105 (41) (2001) 9396–9409.
[5] D. Minakov, P. Levashov, V. Fokin, Vibrational spectrum and entropy in simulation of melting, Comput. Mater. Sci. 127 (2017) 42–47.
[6] W.J. Szlachta, A.P. Bartók, G. Csányi, Accuracy and transferability of gaussian approximation potential models for tungsten, Phys. Rev. B 90 (10) (2014) 104108 .
[7] J.R. Boes, M.C. Groenenboom, J.A. Keith, J.R. Kitchin, Neural network and reaxff comparison for au properties, Int. J. Quantum Chem. 116 (13) (2016) 979–987.
[8] S. Sumpter, D. Noid, On the use of computational neural networks for the prediction of polymer properties, J. Therm. Anal. 46 (3–4) (1996) 833–851.
[9] J. Gasteiger, J. Zupan, Neural networks in chemistry, Angew. Chem. Int. Ed. 32 (4) (1993) 503–527.
[10] J. Thomsen, B. Meyer, Pattern recognition of the 1h nmr spectra of sugar alditols using a neural network, J. Magn. Reson. 84 (1) (1989) 212–217.
[11] M. Keil, T.E. Exner, J. Brickmann, Pattern recognition strategies for molecular surfaces: III. Binding site prediction with a neural network, J. Comput. Chem. 25 (6) (2004) 779–789.
[12] D.K. Agrafiotis, W. Cedeno, V.S. Lobanov, On the use of neural network ensembles in QSAR and QSPR, J. Chem. Inf. Comput. Sci. 42 (4) (2002) 903–911.
[13] A. Jain, G. Hautier, S.P. Ong, K. Persson, New opportunities for materials informatics: resources and data mining techniques for uncovering hidden relationships, J. Mater. Res. 31 (8) (2016) 977–994.
[14] S. Lorenz, A. Groß, M. Scheffler, Representing high-dimensional potential-energy surfaces for reactions at surfaces by neural networks, Chem. Phys. Lett. 395 (4–6) (2004) 210–215.
[15] T.B. Blank, S.D. Brown, A.W. Calhoun, D.J. Doren, Neural network models of potential energy surfaces, J. Chem. Phys. 103 (10) (1995) 4129–4137.
[16] B. Cheng, E.A. Engel, J. Behler, C. Dellago, M. Ceriotti, Ab initio thermodynamics of liquid and solid water, Proc. Nat. Acad. Sci. 116 (4) (2019) 1110–1115.
[17] A.P. Bartók, M.C. Payne, R. Kondor, G. Csányi, Gaussian approximation potentials: the accuracy of quantum mechanics, without the electrons, Phys. Rev. Lett. 104 (13) (2010) 136403 .
[18] A.P. Bartók, M.J. Gillan, F.R. Manby, G. Csányi, Machine-learning approach for one- and two-body corrections to density functional theory: applications to molecular and condensed water, Phys. Rev. B 88 (5) (2013) 054104 .
[19] V.L. Deringer, G. Csányi, Machine learning based interatomic potential for amorphous carbon, Phys. Rev. B 95 (2017) 094203, https://doi.org/10.1103/PhysRevB.95.094203.
[20] A.P. Bartók, J. Kermode, N. Bernstein, G. Csányi, Machine learning a general-purpose interatomic potential for silicon, Phys. Rev. X 8 (4) (2018) 041048 .
[21] X. Qian, R. Yang, Temperature effect on the phonon dispersion stability of zirconium by machine learning driven atomistic simulations, Phys. Rev. B 98 (22) (2018) 224108 .
[22] Z. Li, J.R. Kermode, A. De Vita, Molecular dynamics with on-the-fly machine learning of quantum-mechanical forces, Phys. Rev. Lett. 114 (2015) 096405, https://doi.org/10.1103/PhysRevLett. 114.096405.
[23] A.V. Shapeev, Moment tensor potentials: a class of systematically improvable interatomic potentials, Mult. Model. Simul. 14 (3) (2016) 1153–1173.
[24] E. Podryabinkin, A. Shapeev, Active learning of linearly parametrized interatomic potentials, Comput. Mat. Sci. 140 (2017) 171–180.
[25] K. Gubaev, E.V. Podryabinkin, G.L.W. Hart, A.V. Shapeev, Accelerating high-throughput searches for new alloys with active learning of interatomic potentials, Comput. Mater. Sci. 156 (2019) 148–156, https://doi.org/10.1016/j.commatsci.2018.09.031 URL:http://www.sciencedirect.com/science/article/pii/S0927025618306372.
[26] M. Jafary-Zadeh, K. Khoo, R. Laskowski, P. Branicio, A. Shapeev, Applying a machine learning interatomic potential to unravel the effects of local lattice distortion on the elastic properties of multi-principal element alloys, J. Alloys Compounds, https://doi.org/10.1016/j.jallcom.2019.06.318.
[27] I. Novoselov, A. Yanilkin, A. Shapeev, E. Podryabinkin, Moment tensor potentials as a promising tool to study diffusion processes, 2018.
[28] I.S. Novikov, Y.V. Suleimanov, A.V. Shapeev, Automated calculation of thermal rate coefficients using ring polymer molecular dynamics and machine-learning interatomic potentials with active learning, PCCP 20 (46) (2018) 29503–29512, https://doi.org/10.1039/C8CP06037A arXiv:1805.11924.
[29] P. Souvatzis, O. Eriksson, M. Katsnelson, S. Rudin, The self-consistent ab initio lattice dynamical method, Comput. Mater. Sci. 44 (3) (2009) 888–894.
[30] S. Xiang, F. Xi, Y. Bi, J. Xu, H. Geng, L. Cai, F. Jing, J. Liu, Ab initio thermodynamics beyond the quasiharmonic approximation: W as a prototype, Phys. Rev. B 81 (1) (2010) 014301 .
[31] O. Hellman, I.A. Abrikosov, S.I. Simak, Lattice dynamics of anharmonic solids from first principles, Phys. Rev. B 84 (18) (2011) 180301 .
[32] O. Hellman, P. Steneteg, I.A. Abrikosov, S.I. Simak, Temperature dependent effective potential method for accurate free energy calculations of solids, Phys. Rev. B 87 (10) (2013) 104111 .
[33] J. Dickey, A. Paskin, Computer simulation of the lattice dynamics of solids, Phys. Rev. 188 (3) (1969) 1407.
[34] P. Korotaev, M. Belov, A. Yanilkin, Reproducibility of vibrational free energy by different methods, Comput. Mat. Sci. 150 (2018) 47–53.
[35] G. Kresse, J. Furtmuller, Efficient iterative schemes for ab initio total-energy calculations using a plane-wave basis set, Phys. Rev. B 54 (1996) 11169–11186.
[36] G. Kresse, J. Furthmuller, Efficiency of ab-initio total energy calculations for metals and semiconductors using a plane-wave basis set, Comput. Mat. Sci. 6 (1996) 1–50.
[37] S. Plimpton, Fast parallel algorithms for short-range molecular dynamics, J. Comp. Phys. 117 (1) (1995) 1–19.
[38] C.L. Woodard, X-ray Determination of Lattice Parameters and Thermal Expansion Coefficients of Aluminum, Silver and Molybdenum at Cryogenic Temperatures, University of Missouri-Rolla, 1969.
[39] N. Ashcroft, N. Mermin, Solid State Physics, first ed., Brooks Cole, 1976.
[40] G. Chaudron, Monographies sur les métaux de haute pureté, Masson, 1972.
[41] A. Wilson, R. Rundle, The structures of uranium metal, Acta Crystal. 2 (2) (1949) 126–127.
[42] I. Kruglov, O. Sergeev, A. Yanilkin, A.R. Oganov, Energy-free machine learning force field for aluminum, Sci. Rep. 7 (1) (2017) 8512.
[43] R. Stedman, G. Nilsson, Dispersion relations for phonons in aluminum at 80 and 300 k, Phys. Rev. 145 (2) (1966) 492.
[44] P. Söderlind, B. Grabowski, L. Yang, A. Landa, T. Björkman, P. Souvatzis, O. Eriksson, High-temperature phonon stabilization of γ-uranium from relativistic first-principles theory, Phys. Rev. B 85 (6) (2012) 060301 .
[45] J. Bouchet, F. Bottin, High-temperature and high-pressure phase transitions in uranium, Phys. Rev. B 95 (5) (2017) 054113 .
[46] M. Manley, B. Fultz, R. McQueeney, C. Brown, W. Hults, J. Smith, D. Thoma, R. Osborn, J. Robertson, Large harmonic softening of the phonon density of states of uranium, Phys. Rev. Lett. 86 (14) (2001) 3076.
[47] A. Antropov, K. Fidanyan, V. Stegailov, Phonon density of states for solid uranium: accuracy of the embedded atom model classical interatomic potential, J. Phys.: Conf. Ser. (2018) 012094 Vol. 946, IOP Publishing.
[48] C.D. Taylor, Evaluation of first-principles techniques for obtaining materials parameters of α-uranium and the (001)α-uranium surface, Phys. Rev. B 77 (9) (2008) 094119 .
[49] A. Woods, S. Chen, Lattice dynamics of molybdenum, Sol. St. Commun. 2 (8) (1964) 233–237.
[50] Z.-Y. Zeng, C.-E. Hu, L.-C. Cai, X.-R. Chen, F.-Q. Jing, Lattice dynamics and thermodynamics of molybdenum from first-principles calculations, J. Phys. Chem. B 114 (1) (2009) 298–310.
[51] W. Petry, A. Heiming, J. Trampenau, M. Alba, C. Herzig, H. Schober, G. Vogl, Phonon dispersion of the bcc phase of group-iv metals. I. bcc titanium, Phys. Rev. B 43 (13) (1991) 10933.
[52] B. Grabowski, Y. Ikeda, F. Körmann, C. Freysoldt, A.I. Duff, A. Shapeev, J. Neugebauer, Ab initio vibrational free energies including anharmonicity for multicomponent alloys, arXiv preprint arXiv:1902.11230.
[53] I.S. Novikov, A.V. Shapeev, Improving accuracy of interatomic potentials: more physics or more data? A case study of silica, Mater. Today Commun. 18 (2019) 74–80, https://doi.org/10.1016/j.mtcomm.2018.11.008.